A&A manuscript no.
(will be inserted by hand later)

Your thesaurus codes are:
09 (02.01.4; 02.12.1; 06.01.1; 06.16.2)

ASTRONOMY
AND
ASTROPHYSICS
8.12.1997

Non-LTE analysis of neutral magnesium in the solar atmosphere

G. Zhao[1,2], **K. Butler**[1], **and T. Gehren**[1]

[1] Institut für Astronomie und Astrophysik der Universität München, Scheinerstr. 1, 81679 München, Germany
[2] Beijing Astronomical Observatory, Chinese Academy of Sciences, 100080 Beijing, China

Received date; accepted date

Abstract. We investigate the formation of neutral magnesium lines in the solar photosphere with an atomic model containing 83 levels plus the ground state of Mg II connected via radiative and collisional interactions. Synthetic line flux and intensity profiles are compared with the solar spectrum to study the relevant physical processes and their influence on the level populations and line profiles. For neutral magnesium with the photoionization edges of its three lowest states at $\lambda\lambda$1620, 2514 and 3757 Å the reduction of the ultraviolet radiation field due to metallic line absorption has been taken into account using Kurucz' (1992) ODF opacities. In the photosphere of a cool star excitation and ionization due to collisions with neutral hydrogen can outweigh electron collisions. Therefore the influence of different types of collisional interactions with electrons and neutral hydrogen atoms is examined.

General agreement with solar line profiles in the visible *and* infrared is found for an atomic model with both electron collisions and strongly reduced but significantly large neutral hydrogen collision rates. Our investigation thus extends previous results to lines of all different excitation energies. The atomic model found from the analysis of the solar spectrum will serve as a reference for the investigation of cool metal-poor stars in which both the reduced electron collision rates and the enhanced UV intensities lead us to expect more pronounced deviations from LTE.

Key words: Atomic processes – Lines: formation – Sun: abundances – Sun: photosphere

1. Introduction

The determination of the abundances of the light elements in stars of differing metallicities is important for understanding the chemical evolution of the Milky Way. The first stellar generations are supposed to produce mostly α-elements during massive supernova events of type II. This is observed as a supersolar Mg/Fe abundance ratio in very metal-poor stars, [Mg/Fe] = +0.3 . . . 0.4 and has been reported by a number of researchers (Wallerstein 1961; Gratton & Sneden 1987; Magain 1987; Hartmann & Gehren 1988; Fuhrmann et al. 1995; McWilliam et al. 1995). Studies of α-element synthesis in SNe II have recently been undertaken by Thielemann et al. (1996), Arnett (1991), and Woosley & Weaver (1995). Due to small differences in the way stellar winds and semi-convection are treated and in the specification of the *mass cut* and explosion mechanism their predictions differ, mainly because of differences in the respective Fe yields but also due to non-negligible differences in the pre-explosion yields of Mg. There is no question that Mg, in principle, is less affected by the fine-tuning of SN II explosions. Therefore, inasmuch as the products of SN II nucleosynthesis are mixed into interstellar space ^{24}Mg should constitute a reliable reference of the early evolutionary time scale of the Galaxy.

Due to the number of strong absorption lines found in the visible spectra of even the more metal-poor stars, neutral magnesium is easier to observe than e.g. O I. However, it shares the disadvantage of most neutral metals in the atmospheres of moderately cool stars, with Mg II being the dominant ionization stage above $\approx$ 5000 K. Consequently, neutral Mg I is sensitive to deviations from *local thermodynamic equilibrium*, particularly as its ionization balance is dominated by photoionization from the 3p ^{3}P^o state. In metal-poor cool stars most of the free electrons have vanished and the collision rates are correspondingly smaller. Together with an increased UV radiation field that leads to large photoionization rates this makes Mg I even more sensitive to non-LTE and affects any careful abundance analysis of Mg in these objects. The question then is: when do such deviations from LTE become important? An analysis of the *solar spectrum* will enable us to answer this question.

Several studies have been carried out analyzing the Mg I spectrum in the solar atmosphere starting with the non-LTE analysis of Athay & Canfield (1969) and the LTE analysis of intercombination line formation by Altrock & Cannon (1972). Lambert & Luck (1978) determined the Mg abundance of the solar photosphere assuming LTE and using the Holweger & Müller (1974) model with a constant, isotropic microturbulent velocity ξ_t = 1.0 km/s.

A non-LTE study of the solar Mg I emission lines near 12 μm was published by Lemke & Holweger (1987) who analyzed

Send offprint requests to: T. Gehren

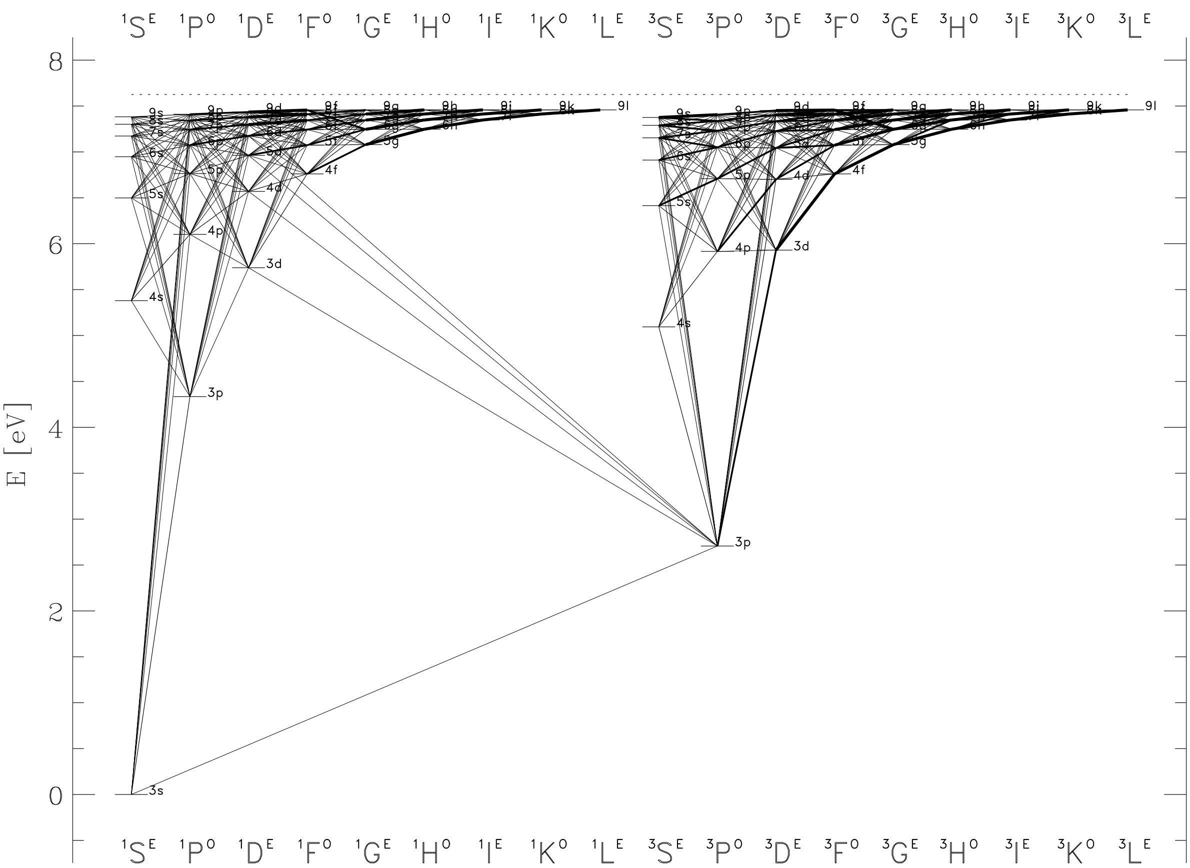

Fig. 1. Mg I Grotrian diagram including all permitted and a few important intercombination radiative bound-bound transitions considered in this paper. The atomic model is complete for n ≤ 9, $\ell \leq$ n $- 1$

the statistical equilibrium of Mg I and the influence of various input data on the line profile. The Mg I model atom they used includes 38 bound levels and 62 line transitions. Their standard non-LTE calculations did not reproduce the emission in the infrared lines. Mauas et al. (1988) used a twelve level atomic model for Mg I line synthesis. They investigated how the computed profiles at λ4571Å and λ5173Å are influenced by the model atom and the choice of its parameters. Carlsson et al. (1992) have explained the formation of the emission lines of Mg I in the solar spectrum near 12 μm employing standard plane-parallel non-LTE line formation with a radiative-equilibrium model atmosphere. They obtained excellent agreement with the observational constraints from a comprehensive atomic model. Although they neglected inelastic collisions with neutral hydrogen particles they were able to reproduce the IR emission line profiles. Recent work on the Mg I non-LTE problem comes from Mashonkina et al. (1996) who explored the corresponding abundance variations in cool stars.

In our present study, we carefully check the various *unblended* Mg I lines visible in the solar spectrum over a wavelength range extending from the blue to the far infrared. All Mg I lines considered here are reproduced using standard non-LTE line formation techniques with the radiative transfer solved in the Auer-Heasley scheme (DETAIL; Giddings, 1981, Butler & Giddings, 1985), taking the population processes between all levels of the Mg model atom into account. The principal aim is not merely to reproduce the observed solar spectrum but also to gather empirical information about the interplay between electron or heavy particle collisions and photoionization.

It is appropriate here to point out that we cannot hope to provide the reader with new results about the *physics* inherent to atomic parameters as inferred e.g. from theoretical considerations or laboratory experiments. It is obvious that the solar atmosphere is more complex in structure than any laboratory plasma; therefore a bad representation of an atmospheric model such as the plane-parallel hydrostatic approach inevitably produces may well mimic details of the interaction processes used in either LTE or NLTE spectrum synthesis. There is, however, reasonable evidence from comparing synthesized and time-integrated observed solar spectra that semi-empirical fits to atomic data such as collision cross-sections indicate some trends that have not yet been predicted by either theoretical atomic physics or terrestrial laboratories. With this in mind we have to employ our model of the solar atmosphere as the single access to atomic data that have not been determined otherwise. Note also that our aim to use both atomic and atmospheric models to analyze magnesium in other stars requires that we model the solar magnesium spectrum with the same set of approximations.

2. Atomic model

The Grotrian diagram of the Mg I model is shown in Fig. 1. We include all levels nℓ up to n = 9 and $\ell \leq$ n $-$ 1 which results in a total of 83 Mg I terms. The model is completed by the doublet ground state of Mg II. All energies were taken from the compilation of Martin & Zalubas (1980) except for those terms with $\ell > 5$ which were obtained using the polarisation formula of Chang & Noyes (1983). Fine structure splitting has been neglected. This model is nearly the same as that used by Carlsson et al. (1992).

2.1. Radiative transition data

The bound-bound transition probabilities for allowed radiative transitions with n $\leq$ 9 and $\ell \leq$ 5 were taken from the Opacity Project (Butler et al., 1993). For the remaining transitions we use Coulomb approximation results according to Bates & Damgaard (1949). The accuracy of the transition probabilities is estimated to be quite high, with errors $\leq$ 10%. We only consider a few important intercombination transitions. The oscillator strength of 3s ^{1}S – 3p ^{3}P^o was taken to be the mean value of that of Wiese et al. (1969) and the recent calculation of Moccia & Spizzo (1988). 3p ^{3}P^o – 3d ^{1}D , 4d ^{1}D, 5d ^{1}D, 6d ^{1}D were taken from Kurucz & Peytremann (1975).

The photoionization cross-sections of the lowest three levels, namely 3s ^{1}S, 3p ^{3}P^o and 3p ^{1}P^o were fitted using an exponential power law to the theoretical calculations of Butler et al. (1993). The resulting photoionization cross-sections of 3s ^{1}S, 3p ^{3}P^o and 3p ^{1}P^o at threshold are 2.5 MB, 17.5 MB and 150 MB respectively; the theoretical cross-sections are displayed in Fig. 2. We thus ignore the explixit influence of the resonances. Consequently, the corresponding *photoionization rates* obtained by a power law approximation are systematically smaller by values of only 16.5%, 7.4%, and 17.8%, respectively, at all optical depths throughout the atmosphere. This introduces no significant errors in both departure coefficients and line profiles mostly because the wavelength region blueward of 2078Å is dominated by opacity from Al I. For longer wavelengths, the simple fits provide a reasonable approximation to the cross sections.

The quantum defect formulae of Peach (1967) are used to determine the photoionization cross sections for n $\leq$ 7 and $\ell \leq$ 3. For all other levels the hydrogenic approximation is used.

2.2. Collisional transition data

2.2.1. Electron collisions

The cross-sections of the *allowed* transitions for electron impact excitation were computed following van Regemorter's (1962) formula. The mean gaunt factor g in the formula was set equal to 0.2 if the principal quantum number n changes in the transition and to 0.7 if it does not. When van Regemorter's formula is compared with the electron impact excitation (Seaton 1962), it turns out that the latter is systematically smaller. Mashonkina (1996) has shown that for Mg I differences up to a factor of 100 do occur, however, with a line-to-line scatter of similar amplitude. Our comparatively high values for *allowed* electron collisions may therefore represent an upper limit towards level thermalization. Any smaller collision rates will change the departure coefficients towards stronger non-LTE effects. The cross-sections of the *forbidden* transitions for electron impact excitation were computed from the semi-empirical formula of Allen (1973), in which the collision strength is set equal to 1 for all transitions. Here, Mashonkina (1996) shows that calculations using the Born approximation may lead to significantly greater collision cross-sections, in particular for transitions between highly excited levels with small energy separation. Our choice therefore may imply that our *forbidden* electron collision rates are systematically low. We note that there is no simple argument that could assist in the proper choice of the electron collision rates, and we return to this problem when discussing the infrared emission lines. The cross-sections for electron impact ionization were calculated using the formula of Seaton (1962) for energy levels up to n $\leq$ 9 and $\ell \leq$ 5, since their photoionization cross-sections at threshold were available. For the few high ℓ value levels a semi-empirical formula (Drawin 1969) was employed.

2.2.2. Collisions with hydrogen atoms

Excitation and ionization by inelastic collisions with heavy particles are often considered to be unimportant compared with electron collisions since they have much smaller cross-sections (Omont 1977, Petitjean & Gounand 1984, Carlsson et al. 1992, Caccin et al. 1993). However, taking the larger number density of neutral hydrogen in the solar photosphere into account, the collision *rates*, could be of interest in cases where the statistical equilibrium depends sensitively on collisions. Thus some investigators consider this kind of collision to be very important (e.g. Steenbock 1985, Lemke & Holweger 1987) since the ratio of number densities $N_{\rm H}/N_e$ in cool stars may easily exceed 10^4. Baumüller & Gehren (1996) in their analysis of the solar aluminium line formation encountered a similar case. They applied the hydrogen collision formula as derived by Drawin (1969) but allowing for a *scaling factor* $S_{\rm H}$ that varied in an almost step-like fashion at some excitation energy E_n. We carefully investigated the influence of hydrogen collisions in our atomic model by fitting all available Mg I lines. As for the Al I atom we again had to modify Drawin's formula by a scaling factor.

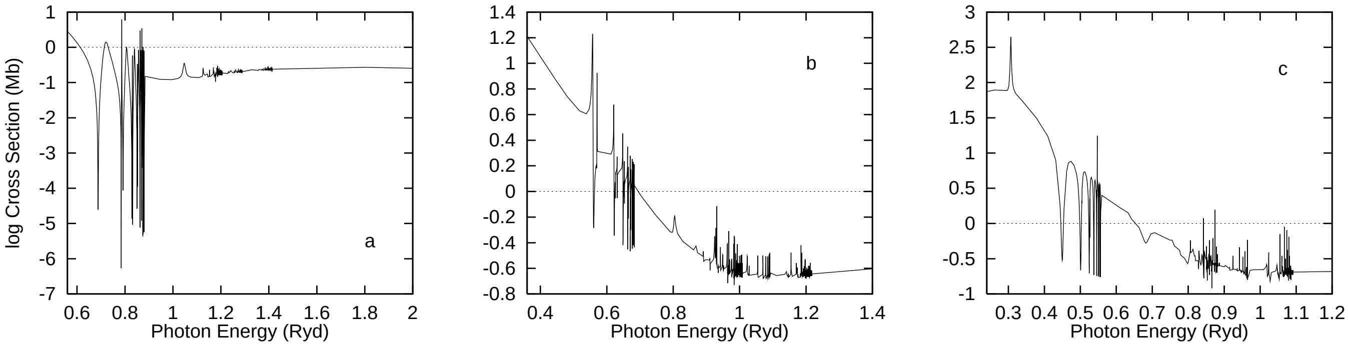

Fig. 2. Mg I photoionization cross-sections for the three lowest terms (Butler et al. 1993). The edges are near a: 1620 Å (3s ^{1}S,); b: 2514 Å (3p ^{3}P^o); and c: 3757 Å (3p ^{1}P^o).

However, for Mg I the factor varies *exponentially* with upper level excitation energy $E_{\rm n}$ (in eV),

$$S_{\rm H} = 1000 \times e^{-{\rm n}E_{\rm n}/2} \quad .$$

This was determined in a fully empirical manner, recomputing the complete non-LTE line formation with statistical equilibrium equations including the differing hydrogen collision rates, and it enabled us to fit lines of different excitation energies. The notion of hydrogen collision cross-sections decreasing systematically with excitation energy is also in rough agreement with Kaulakys' (1985, 1986) prediction for Rydberg transitions. Although Lemke & Holweger (1992) were unable to reproduce the infrared Mg I *emission lines* using the Holweger-Müller model atmosphere they point out that the emission lines may require hydrogen collision cross-sections that depend on the excitation energy of the lower level of a transition. This trend seems to compensate the very rough approximation of the atomic collisions in a similar way in both Al I and Mg I. The consequences of this particular form of the hydrogen collision rates will be discussed in Sect. 5.

3. Model atmospheres

The statistical equilibrium calculations are performed in horizontally homogeneous LTE model atmospheres in hydrostatic equilibrium. We account for metallic and molecular UV line absorption using Kurucz' (1992) opacity distribution functions interpolated for the proper solar mix of abundances. The solar abundances are adopted from Holweger (1979) with minor modifications for carbon (Stürenberg & Holweger 1990). For Fe and Mg we use values of 7.51 and 7.58, respectively. Four different solar temperature stratifications are explored for comparison. The first model in Fig. 3, labeled GRS88, is flux-conserving, convection is taken into account parametrically with a mixing-length of 0.5 pressure scale heights (Fuhrmann et al. 1993) and line blanketing included with Kurucz' ODFs. This is our *standard* solar model atmosphere although we are aware that it does not reproduce the centre-to-limb variation of the solar continuum intensities very well. The reason for adopting this model as a standard is that we can easily use the model as a differential *stellar* atmosphere with full physics included. This does not hold for the second type of solar model in Fig. 3, labeled HM74, which is the semi-empirical model of Holweger & Müller (1974). As was shown by Fuhrmann et al. (1993, 1994) scaled semi-empirical temperature stratifications should not be used for stars with parameters very different from the Sun; this is particularly important for metal-poor stars. Experience with the two solar temperature stratifications shows that they are both able to reproduce most of the line flux spectra provided that abundances and damping constants are properly adjusted. The third model in Fig. 3, labeled EAGLNT93, is a theoretical convective equilibrium model from the Uppsala group and their co-workers (Edvardsson et al. 1993). It was calculated with opacity sampling including millions of lines from the compilation of Kurucz (1990). The final model in Fig. 3, labeled MACKKL86, is the empirical model constructed at Harvard by Avrett and his co-workers (Maltby et al. 1986). They include more opacity from the ultraviolet lines that were later published by Kurucz (1990), which results in a less steep photospheric temperature gradient because the increase in the quasi-continuous *line-haze* opacity shifts the computed heights of formation of the observed ultraviolet continua outwards (Rutten 1988). Model MACKKL obviously differs from the other three models at greater heights by a chromosphere with a steep temperature rise.

In the context of fitting the Mg I lines considered here, we have made test calculations with the four models. Experience with these solar temperature stratifications shows that all of them are able to reproduce most of the line flux spectra provided that abundances and damping constants are properly adjusted. The abundance differences between the LTE and non-LTE calculations have nearly the same value for all four models even though we had to adjust some line parameters (e.g. $\log C_6$, $\log gf$) in order to obtain a better line fit.

3.1. Statistical equilibrium calculations

The statistical equilibrium is calculated using the DETAIL code (Giddings 1981; Butler & Giddings 1985) in a version based on the method of complete linearization as described by Auer

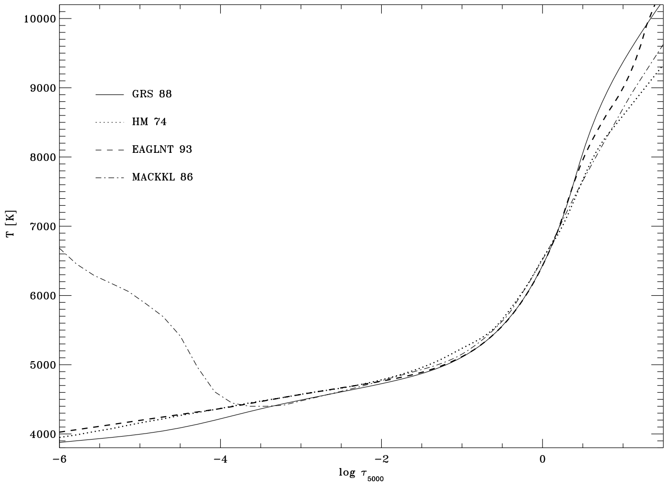

Fig. 3. Comparison of different solar model atmospheres, the ODF-blanketed model used here (GRS88), the Holweger-Müller model (HM74), the Edvardsson et al. (1993) opacity sampling model (EAGLNT93), and the Maltby et al. (1986) empirical model (MACKKL86)

Table 1. Atomic data for Mg I line synthesis

λ [Å]	transition	E_{low} [eV]	E_{up} [eV]	$\log gf$	$\log C_6$
4571.096	3s ^{1}S – 3p ^{3}P^o	0.00	2.70	−5.690	−31.25
4730.029	3p ^{1}P^o – 6s ^{1}S	4.33	6.94	−2.290	−29.12
5711.091	3p ^{1}P^o – 5s ^{1}S	4.33	6.49	−1.724	−30.18
11828.19	3p ^{1}P^o – 4s ^{1}S	4.33	5.37	−0.333	−30.10
4702.990	3p ^{1}P^o – 5d ^{1}D	4.33	6.95	−0.377	−29.88
5528.409	3p ^{1}P^o – 4d ^{1}D	4.33	6.56	−0.498	−30.35
8806.770	3p ^{1}P^o – 3d ^{1}D	4.33	5.73	−0.215	−31.03
8213.020	3d ^{1}D – 6f ^{1}F^o	5.73	7.23	−0.509	−29.15
8923.570	4s ^{1}S – 5p ^{1}P^o	5.37	6.75	−1.580	−29.38
5167.322	3p ^{3}P^o – 4s ^{3}S	2.70	5.09	−0.876	−30.86
5172.697	3p ^{3}P^o – 4s ^{3}S	2.70	5.09	−0.399	−30.86
5183.620	3p ^{3}P^o – 4s ^{3}S	2.70	5.09	−0.177	−30.88
7657.600	4s ^{3}S – 5p ^{3}P^o	5.09	6.70	−1.178	−29.90
6318.750	4s ^{3}S – 6p ^{3}P^o	5.09	7.04	−1.952	−29.05
6319.240	4s ^{3}S – 6p ^{3}P^o	5.09	7.04	−2.201	−29.05
6319.493	4s ^{3}S – 6p ^{3}P^o	5.09	7.04	−2.679	−29.05
122240.8*	6g – 7h	7.27	7.37	1.9207	−29.96
123217.3*	6h – 7i	7.27	7.37	2.1574	−30.06

* lines at 12.2 and 12.3 μm were both computed with $\log C_4 = -9.8$

& Heasley (1976). The calculation includes all radiative line transitions which are mostly represented by Doppler profiles; 99 lines were linearized. The Mg b lines are treated with full radiative and van der Waals damping. The linearized line transitions were selected from test calculations including different combinations with a preference for the stronger transitions including the ℓ = n − 1 levels. Adding more transitions did not change the results. The bound-free transitions of the lowest 22 levels were linearized, too.

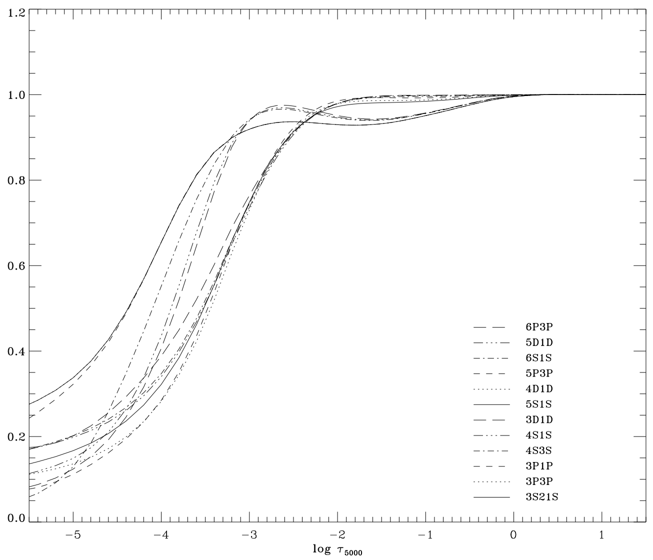

Fig. 4. Departure coefficients b_n for some levels of Mg I in the solar atmospheric model GRS88.

3.2. Background opacities

In a star such as the Sun the flux in the ultraviolet spectral region is determined to a large part by opacities due to metal line absorption. We again use the opacity distribution functions of Kurucz (1992) to represent this opacity. In these ODF data single line opacities in small frequency intervals are represented by superlines; consequently, the ODF opacity is not identical to that required at a specific position in frequency space. For the calculation of a model atmosphere this simplification is a sufficient approximation, but for non-LTE line formation the actual radiation field across a line transition or an ionization continuum is important for the determination of the statistical equilibrium of an atom. For bound-free transitions the exact position of the absorbing lines is less important, and the use of the ODFs will be reliable, provided the intervals are small enough in the frequency region near the ionization edge. For a bound-bound transition with its narrow line width it can be important in which part of the broad synthetic ODF line it is formed. We include the additional ODF opacity in the UV for wavelengths between 1300 and 3860 Å to allow for a realistic behaviour of the ionization from the ground state and the first excited level without affecting most of the line transitions. Only a few Mg I lines are found in this region allowing us to omit additional line opacities as most of these transitions are of minor importance for the statistical equilibrium.

4. Results

The statistical equilibrium of Mg I in the solar photosphere is similar to that found for Al I (Baumüller & Gehren 1996). This is not unexpected since both atomic systems are dominated by their low-level photoionization in the UV. In fact, taking into account that Mg I is mainly photoionized from the triplet ground state which is connected to the singlet ground state by an *intercombination line* whereas Al I is photoionized directly from its ground state, the similarity in the population pattern found for the levels of different excitation is striking. The *completeness* of the atomic model has been investigated with a variety of different model atoms, and the result is the atomic model presented in Fig. 1. Additional tests were devoted to the formulation of the hydrogen collision rate scaling factor $S_{\rm H}$. The results refer to the following models,

(A) LTE populations
(B) statistical equilibrium with hydrogen collisions according to the original formula of Drawin (1969), and
(C) statistical equilibrium with hydrogen collisions from Drawin (1969) but scaled exponentially with upper level excitation energy as described in Sect. 2.2.2.
(D) statistical equilibrium with no hydrogen collisions

Model (C) is the non-LTE reference model which is our standard unless stated otherwise. Its implications will be discussed in more detail below (see Sect. 5).

4.1. Departure coefficients

Fig. 4 shows the typical run of some of the more important level populations with optical depth. Here, the departure coefficients are defined as usual as the ratio $b_n = N_n/N_n^{\rm LTE}$ between statistical equilibrium and thermal (Saha-Boltzmann) number densities. Note that in spite of relatively strong collisional interaction – including neutral hydrogen atoms – all level populations already deviate from their LTE values at optical depths near unity. This underpopulation is the result of the large photoionization rate which is known to dominate the near-UV spectra of cool stars such as the Sun. It is important to recognize that the deviations among the departure coefficients of different levels are reduced by increasing the contributions of the *hydrogen collisions*. Such effects as well as corresponding changes of the *electron collisions* have been discussed by Baumüller & Gehren (1996).

4.2. Line profiles

The synthetic line profiles shown in Figs. 5 and 6 are all calculated on the basis of the standard line data set used also for the determination of the statistical equilibrium (*cf.* Table 1). The lines are compared with solar flux observations taken from the Kitt Peak Atlas (Kurucz et al. 1984) and with solar intensity profiles at three disc positions from the infrared atlases of Farmer & Norton (1989) and Brault and Noyes (1983).

The synthetic flux profiles have been convolved with a rotation velocity of $v \sin i \;=\; 2$ km/s and a Gaussian macroturbulence distribution of $\Xi_t \;=\; 1.4$ km/s. This profile is derived from a series of fits to solar lines of different strength. Line broadening is partly treated in a semi-empirical mode where the C_6 constants are evaluated from solar line fits. Damping due to the quadratic Stark effect has only been included for the 12 μm IR line profiles. When computing C_4 broadening constants according to the Lindholm theory (*cf.* Hunger 1960), the quadratic Stark effect becomes the dominant source of line broadening for most Mg I transitions involving n $>$ 6, except for S or P terms. This is at variance with the semi-classical impact approximation of Cowley (1971) or Freudenstein and Cooper (1978) which at solar atmospheric temperatures leads to damping parameters roughly an order of magnitude *smaller* (a factor of 15 for the 12 μm line; see also Chang & Schoenfeld 1991 and Dimitrijević & Sahal-Bréchot 1996). Note also that the often used approximation of a *mean* interacting nearby level such as the $< \Delta E_\infty >$ introduced by Freudenstein and Cooper (their eq. (22)) may lead to substantially *smaller* values for C_4 for nearly all levels. For the 7i ^{3}I term the corresponding factor is 600. Whereas in most other transitions van der Waals damping rules, the 12 μm lines are dominated by the quadratic Stark effect for which we have used the values given in Table 1. The same broadening constants were used for all models (A) to (D).

In the following we discuss the properties of selected groups of lines.

4.2.1. Intercombination line

In the solar photosphere the intercombination line of Mg I at 4571 Å has been inferred from NLTE model synthesis to be formed completely under thermal excitation conditions (e.g. Altrock & Cannon 1972; Altrock & Canfield 1974; Mauas et al. 1988). Carlsson et al. (1992) point out that the 4571 Å line is the only line in the optical spectrum of the Sun producing a line centre *emission reversal* at the solar limb (where the line-of-sight crosses the temperature minimum). We confirm that the difference between the LTE and non-LTE line profiles in model (C) with the exponentially scaled hydrogen collisions is negligibly small, corresponding to $\Delta \log \varepsilon = \log \varepsilon_{\rm NLTE} - \log \varepsilon_{\rm LTE} =$ 0.040 dex. As a result of the strong photoionization in the statistical equilibrium the opacity of the intercombination line is reduced by 10 . . . 20%, and the line is therefore formed slightly *deeper* in the atmosphere under non-LTE conditions compared to that calculated assuming LTE. This explains the small difference in the line core and the resulting abundance change evident from Fig. 5.

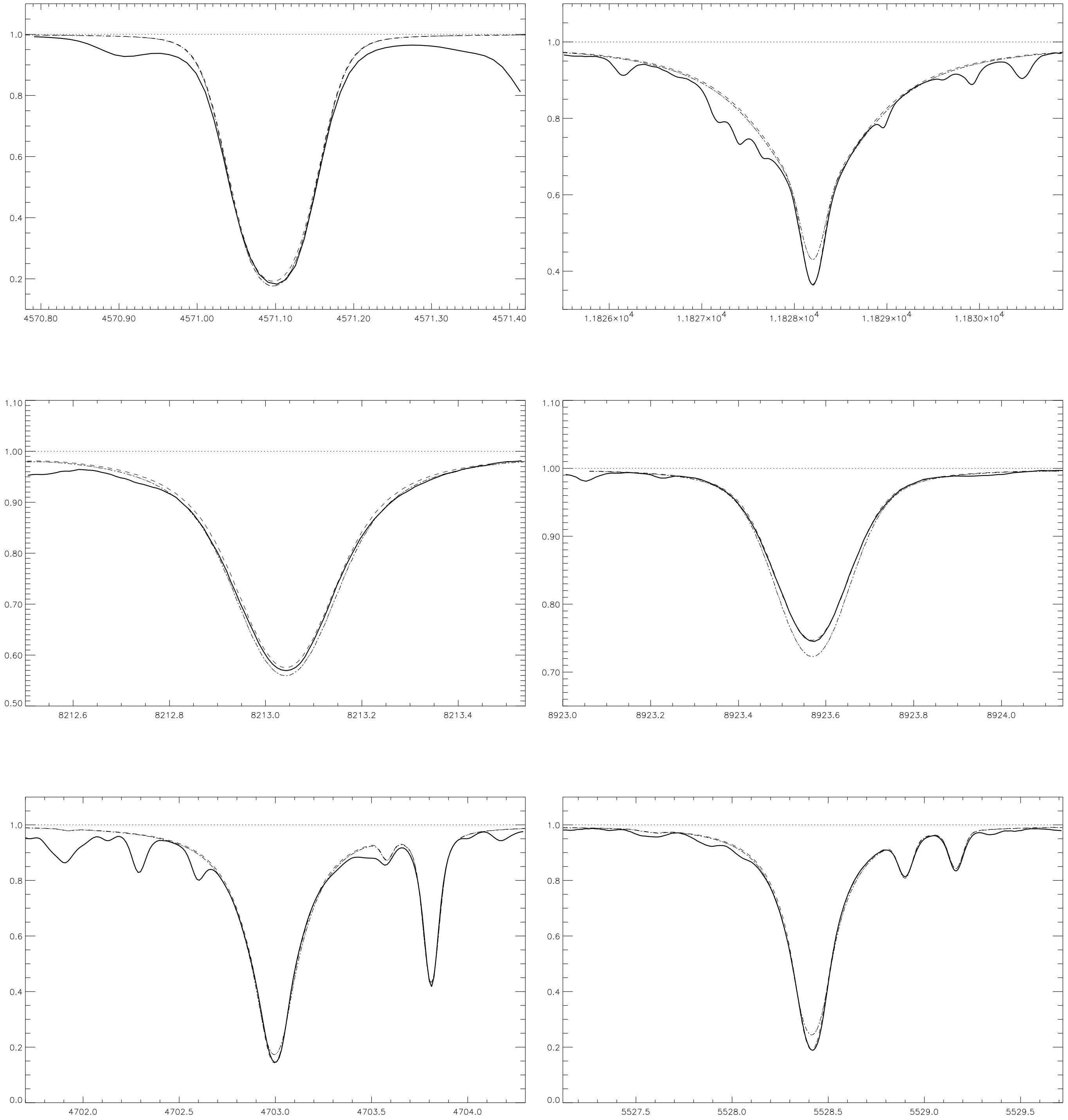

Fig. 5. Synthetic flux profiles of selected Mg I lines compared with the observed spectrum of the Kurucz et al. (1984) solar flux atlas (continuous line). The line profiles refer to LTE (Model A, dot-dashed), and to the final statistical equilibrium model (C) with hydrogen collisions scaled exponentially with excitation energy (dashed). (*top left*): intercombination line 3s ^{1}S – 3p ^{3}P^o at 4571 Å. (*top right*): excited line 3p ^{1}P^o – 4s ^{1}S at 11828 Å. (*middle left*): 3d ^{1}D – 6f ^{1}F^o transition at 8213 Å. (*middle right*): excited line (4s ^{1}S – 5p ^{1}P^o) at 8923 Å. (*bottom left*): 3p ^{1}P^o – 5d ^{1}D transition at 4703 Å. (*bottom right*): 3p ^{1}P^o – 4d ^{1}D transition at 5528 Å.

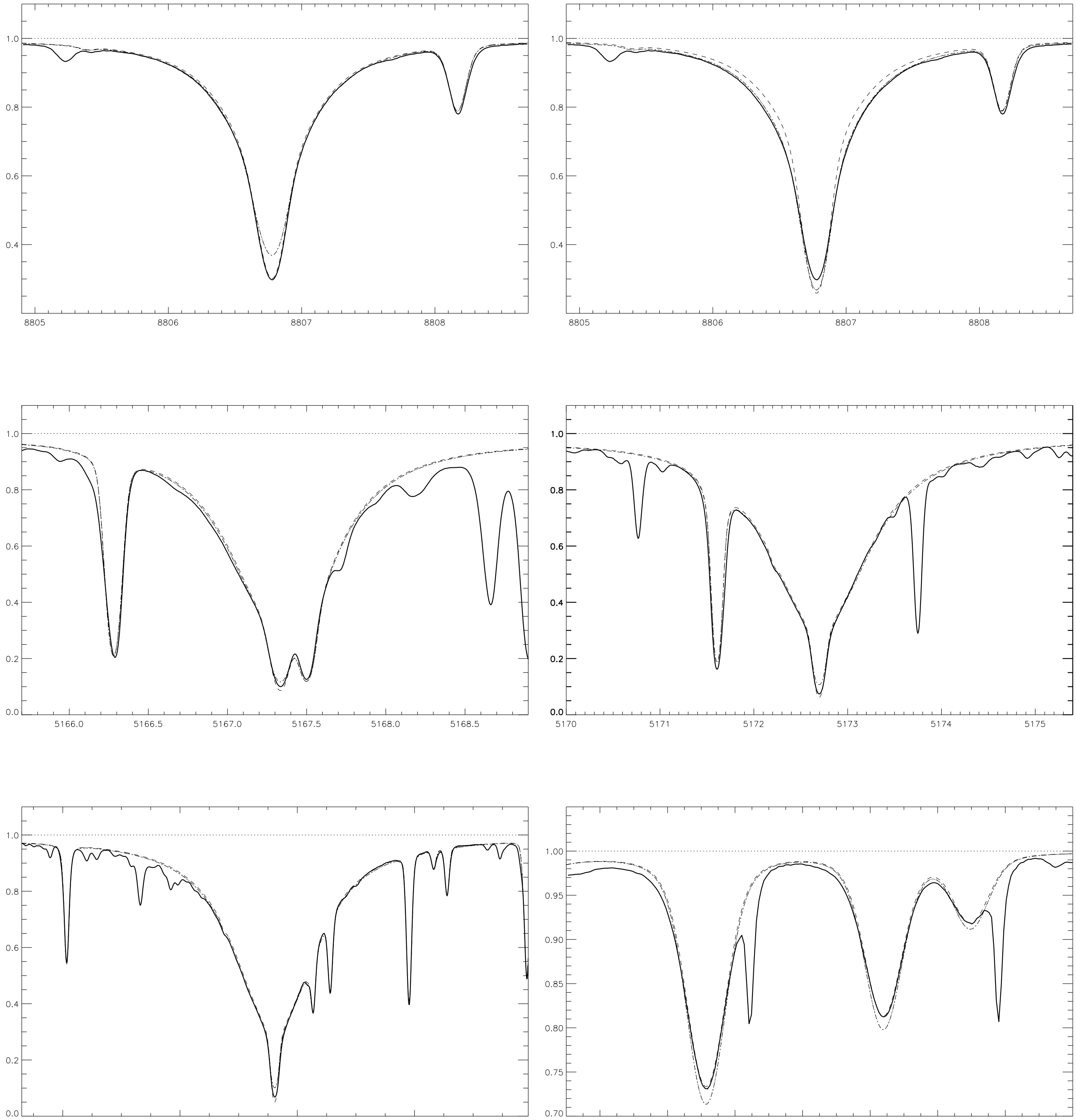

Fig. 6. Synthetic flux profiles of selected Mg I lines compared with the observed spectrum of the Kurucz et al. (1984) solar flux atlas (continuous line). (*top*): 3p ^{1}P$^{\mathrm{o}}$ – 3d ^{1}D transition at 8806 Å. (*left*): line profiles for LTE and non-LTE reference model (C). (*right*): line profiles for non-LTE model with hydrogen collisions according to Drawin's (1969) original formula (model B, dot-dashed), and with no hydrogen collisions (model D, dashes). All other line profiles refer to LTE (Model A, dot-dashed), and to the final statistical equilibrium model (C) with hydrogen collisions scaled exponentially with excitation energy (dashed). (*middle left*): Mg I b line (3p ^{3}P$^{\mathrm{o}}$ – 4s ^{3}S) at 5167 Å including strong Fe blend. (*middle right*): Mg I b line at 5172 Å. (*bottom left*): Mg I b line at 5183 Å. (*bottom right*): 4s ^{3}S – 6p ^{3}P$^{\mathrm{o}}$ triplet near 6319 Å

4.2.2. Excited lines

Inspection of the synthetic line profiles displayed in Figs. 5 and 6 reveals that — mainly as a consequence of decoupling of the level populations due to the strong photoionization — the excited Mg I lines show quite different non-LTE effects, predominantly in the line cores. Whereas most of the lines such as $\lambda\lambda 11828, 4703, 5528$, and 8806 Å have line cores that are *too weak*, those of $\lambda\lambda 8923$ and 6319 Å are *too strong* as compared with the solar flux spectrum. The latter group of lines seems to arise from the more excited levels above 5 eV; therefore they provide an important test for the Mg I atomic model.

11828 Å: The Mg I $\lambda 11828$ Å line displayed in Fig. 5 marks the transition from level 3p ^{1}P^o to 4s ^{1}S. Together with $\lambda\lambda$ 8806 Å and 8923 Å it strongly emphasizes the need to include hydrogen collisions in the Mg I model. Model calculations with *constantly increased electron collision rates* do not produce the necessary run of the departure coefficients since electron collisions are more important in the *inner* part of the photosphere whereas the profile diverges from LTE in the line core which is formed at optical depths around $\tau_c = 0.001$. The explanation for the dominance of hydrogen collisions in these outer regions is buried in the fact that the N_H/N_e density ratio increases by an order of magnitude between $\tau_c = 1$ and $\tau_c = 0.01$. The non-LTE calculation with the exponentially scaled hydrogen collisions (C) thus provides the best fit to the profile (see also the λ 8806 Å line in Fig. 6), and any replacement introducing enhanced *electron* collisions instead would require an *individual adjustment* of many lines which increases the number of free parameters even more. It should also be noted here that *increasing* the electron collision rates will lead *away* from the impact approximation as discussed in section 2. Which of the two alternatives represents the real plasma can in principle be decided by analyses of cool metal-poor stars that have a significantly greater N_H/N_e density ratio in their atmospheres, if the lines under consideration could be observed there. Such an investigation has been followed in the case of Al I (Baumüller & Gehren 1997), and a corresponding analysis is planned for Mg I. The difference in the abundance determination between the LTE and non-LTE calculations amounts only to $\Delta \log\varepsilon = -0.010$ dex, because the deficiency of the LTE profile in the line core is mostly compensated by slightly stronger LTE line wings.

8213 Å: Mg I $\lambda 8213$ Å couples 3d ^{1}D with the 6f ^{1}F level. $\lambda 8213$ Å is similar to $\lambda 8923$ Å and to the 6319 Å triplet in that it displays an LTE line profile that is notably stronger than its non-LTE counterpart. This is a reversal of the behaviour of the 11828 and 8806 Å lines, and Fig. 4 outlines that it is due to the different coupling of the $3d$ and $4s$ terms to the $3p$ terms at lower energies and to the $4p$ and $4f$ terms at higher energies. As explained above the $3s$ and $3p$ terms are depopulated by strong photoionization, however, with *collisonal* coupling becoming less important (a) for optical depths decreasing, and (b) for energy increasing. In particular the coupling to highly excited energy levels is considerably less effective than that between the $3p$ and $4s$ (or $3d$) terms, and there will be a net cascade of electrons that populate the $4s$ and $3d$ terms without fully thermalizing the $3p$ term. However, the 8213 Å line is not only affected at the line core but over a significant fraction of its wings (see Fig. 5). Consequently, the abundances determined from non-LTE and LTE differ by $\Delta \log\varepsilon = 0.073$ dex.

8923 Å: The Mg I $\lambda 8923$ Å line arises from the transition of 4s ^{1}S to 5p ^{1}P. Its line core displays a dominant non- LTE influence. Again, $\lambda 8923$ Å has a deeper LTE line core than that of the non-LTE calculation (see Fig. 5). The abundance difference between non-LTE and LTE results is also large with $\Delta \log\varepsilon = 0.073$ dex.

4703 Å: Mg I $\lambda 4703$ Å couples the first excited singlet level 3p ^{1}P^o with 5d ^{1}D. Though it is not as strong, this line has a similar behaviour to the Mg I b triplet. The $\lambda 4703$ Å profile fit is shown in Fig. 5. The difference between the abundance determinations using either non-LTE or LTE calculations is small, with $\Delta \log\varepsilon = -0.024$ dex.

5528 Å: The Mg I $\lambda 5528$ Å line marks the transition from 3p ^{1}P^o to 4d ^{1}D. This line displays a clear increase in the deviation from LTE at the line core as compared with the 4703 Å line. The $\lambda 5528$ Å profile fit is shown in Fig. 5. The difference between the abundances determined in the non-LTE and LTE calculations is $\Delta \log\varepsilon = -0.020$ dex.

8806 Å: Mg I $\lambda 8806$ Å line is the transition from level 3p ^{1}P^o to 3d ^{1}D, *i.e.* the *leading* line of the singlet $3p$ – nd series. This line therefore shows the strongest deviation from LTE in the line core (see Fig. 6). $\lambda 8806$ Å has an exceptionally strong *isotopic shift*, and the three components corresponding to ^{24}Mg, ^{25}Mg and ^{26}Mg have intensities in the ratio of 10:2:2 with wavelengths at $\lambda\lambda$ 8806.7678, 8806.7358 and 8806.7032 Å , respectively (Meißner 1938). The line plays an important rôle in the determination of the collision rates with neutral hydrogen. We see clearly in Fig. 6 that the Mg I atomic model either without hydrogen collisions (D) or with hydrogen collisions using Drawin's (1969) standard formula (model B) does not fit the observed flux profile. The corresponding scaling factors are S_H = 0 or 1 for models (D) and (B), respectively, but 1.6 for model (C). Since the line core is formed in the uppermost photospheric layers, it is particularly sensitive to collisions, and a factor of 2 in collision rates both thermalizes the line source function near $\log\tau_c$ = -2.5 *and* decreases the line center optical depth thus avoiding strong contributions from upper photospheric layers where the $3d$ departure coefficient falls below that of $3p$. However, the difference in the abundance determinations from the equivalent width using either non-LTE or LTE calculations with model (C) is very small, $\Delta \log\varepsilon = -0.004$ dex.

Mg b triplet: The Mg I b triplet at $\lambda\lambda$ 5167, 5172 and 5183 Å, arises from transitions between the first excited level 3p ^{3}P^o to 4s ^{3}S. These lines are formed from near LTE level populations except for a slight deviation from LTE in the line core; the core, however, cannot be synthesized without introducing a model chromosphere. The line profile fits of the Mg I b lines are reproduced in Fig. 6. The synthetic flux profiles with dot-dashed lines refer to the LTE calculation (model A), whereas the dashed lines are non-LTE calculations with exponentially scaled hydrogen collisions of model (C). The very cores differ from the observed solar flux profiles by approximately 2%.

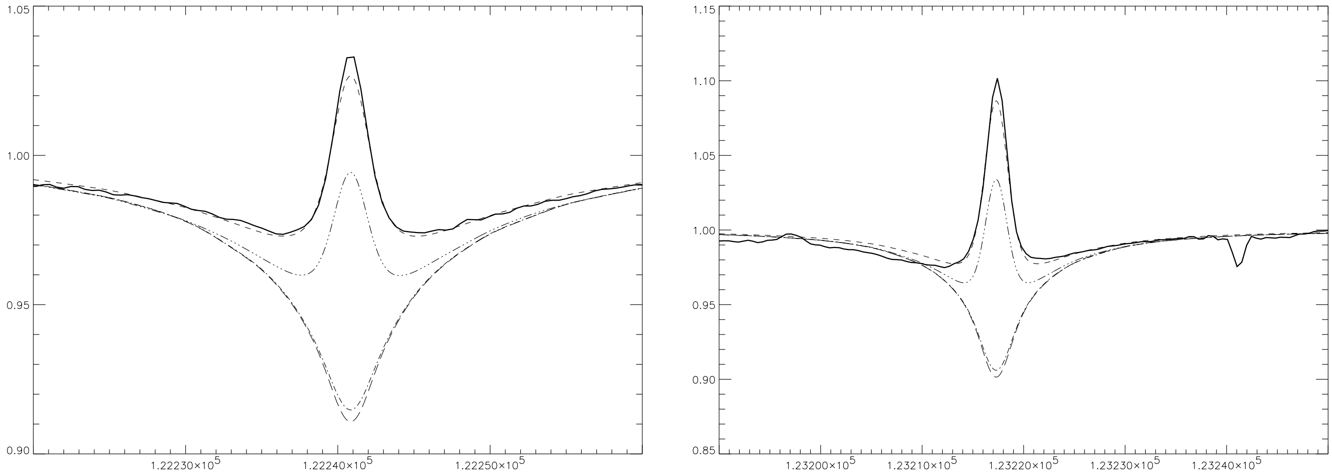

Fig. 7. Line *intensity* profiles of two Mg I Rydberg transitions near 12μm calculated for different atmospheric and atomic models, and compared with the spectrum observed at the centre of the solar disk (Brault & Noyes 1983) (solid line). LTE from GRS88 model atmosphere: long dashes. LTE from HM74 model: dash-dots. Non-LTE model with full hydrogen collisions: dash-three dots. Non-LTE model (C) with exponentially scaled hydrogen collisions: dashes. (*left*): 6g – 7h transition at 12.22 μm. (*right*): 6h – 7i transition at 12.32 μm.

Similar to the Na D lines the *chromospheric* contributions to the line cores therefore may be affected by small-scale velocity fields. The difference in the abundance determinations between non-LTE and LTE calculations amounts to $\Delta \log\varepsilon = -0.019$ dex.

6319 Å triplet: This triplet, arising from the $4s\,^3S$ (*i.e.* the *upper* level of the Mg b lines) to $6p\,^3P$ transition, is located at $\lambda\lambda$ 6318.75, 6319.20 and 6319.43 Å. The λ6319 Å triplet shows abnormal behaviour compared with the other triplet lines since the synthetic LTE flux profile is *deeper* than that of the non-LTE calculation in the central part of the profiles (see Fig. 6). The difference between the abundances determined with LTE or non-LTE calculations amounts to $\Delta \log\varepsilon = 0.048$ dex.

4.2.3. Emission lines near 12μm

The existence of two emission lines in the solar spectrum near 12 μm was announced by Murcray et al. (1981). Chang & Noyes (1983) identified these lines as transitions between highly excited levels of Mg I, 12.2μm or 818.058 cm^{-1} ($3s7h^{1,3}H^o$ – $3s6g^{1,3}G$) and 12.3μm or 811.578 cm^{-1} ($3s7i^{1,3}I$ – $3s6h^{1,3}H^o$), respectively. Brault & Noyes (1983) were the first to study these Mg I lines and demonstrate their large diagnostic potential, with line profile observations from different areas on the solar disk. Carlsson et al. (1992) carried out non-LTE calculations for the Mg I emission lines and they were able to reproduce the emission feature. As was also pointed out by Lemke & Holweger (1992) these lines are formed in the *photosphere*; therefore modelling the chromospheric temperature rise is not required. Even small deviations from LTE of the corresponding level populations create a relative population inversion that produces an outward increase of the line source function sufficient to form an emission profile. The reason lies in the increasing importance of stimulated emission in this wavelength region. A more detailed description of other investigations of these famous Mg I emission lines can be found in Carlsson et al. (1992) and further references therein. Similar lines are found for Al I, and they have been analyzed by Baumüller & Gehren (1996).

The calculated line intensity profiles of the 7h – 6g transition at 12.2 μm and the 7i – 6h transition at 12.3 μm are compared with the spectrum observed at the solar disc centre (Brault & Noyes, 1983) in Fig. 7, from which it can be seen very clearly that LTE synthesis from both the GRS88 model or the HM74 model of course cannot reproduce the Mg I emission feature. The non-LTE calculations with our Mg I model can reproduce the observed 12μm emission peak. While the line fit using neutral hydrogen collisions calculated according to the standard Drawin formula (model B) is not very convincing, we obtain excellent agreement with the observed profile when treating the same collisions with the empirical correction factor to Drawin's formula given in section 2.2.2. A similarly good fit is naturally obtained in this particular case for model (D) since $S_{\rm H} = 0$ is not significantly different from $S_{\rm H} = 3\,10^{-10}$, the value obtained from our hydrogen scaling formula.

The centre-to-limb variation of both line profiles is plotted in Fig. 8. Our fit is exceptionally precise; in fact it is better than that of some of the pure absorption lines. The two lines thus offer a unique opportunity to study the influence of hydrogen collisions in statistical equilibrium systems. The exponential scaling formula proposed in Sect. 2.2.2 is fixed at its upper end (at high excitation energies) by comparison with these Rydberg transitions, and in the middle or at its lower end by transitions such as the 8806 Å line. The exponential scaling of the Drawin (1969) formula produces results similar in quality to the step-like scaling used by Baumüller & Gehren (1996), but it requires

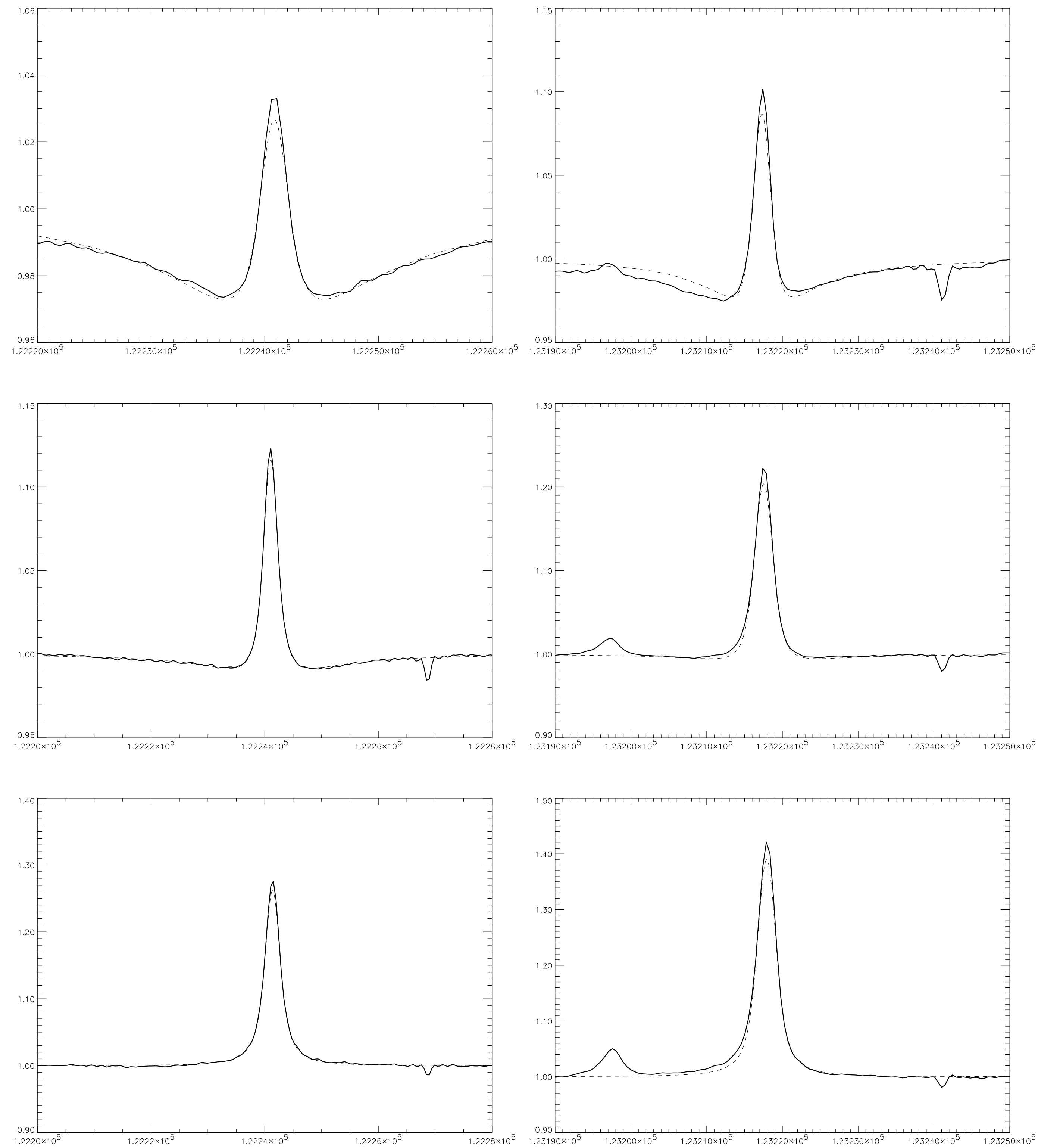

Fig. 8. Centre-to-limb variation of Mg I Rydberg transitions near 12μm comparing the solar observations of Brault & Noyes (1983, solid line) with the profiles arising from the non-LTE model with exponentially scaled hydrogen collisions (dashes). (*left column*): 6g – 7h transition, (*right column*): 6h – 7i transition. From top to bottom the spectra refer to $\mu = 1.0, 0.5$, and 0.2, respectively

Table 2. Comparison of calculations using different atomic models with hydrogen collisions following Drawin's formula (B), exponentially scaled hydrogen collisions (C), and no hydrogen collisions (D)

λ [Å]	transition	$\Delta \log \varepsilon = \log \varepsilon_{\rm NLTE} - \log \varepsilon_{\rm LTE}$ (B)	(C)	(D)
4571.096	$3s\,^1S - 3p\,^3P^o$	0.030	0.040	0.065
4730.029	$3p\,^1P^o - 6s\,^1S$	0.014	0.040	0.078
5711.091	$3p\,^1P^o - 5s\,^1S$	0.020	0.041	0.088
11828.19	$3p\,^1P^o - 4s\,^1S$	−0.020	−0.010	0.045
4702.990	$3p\,^1P^o - 5d\,^1D$	0.004	−0.024	0.056
5528.409	$3p\,^1P^o - 4d\,^1D$	0.000	−0.020	0.060
8806.770	$3p\,^1P^o - 3d\,^1D$	−0.026	−0.004	0.088
8923.570	$4s\,^1S - 5p\,^1P$	0.106	0.017	0.073
8213.020	$3d\,^1D - 6f\,^1F$	0.037	0.011	0.073
5167.322	$3p\,^3P^o - 4s\,^3S$	0.011	−0.019	0.044
5172.697	$3p\,^3P^o - 4s\,^3S$	0.010	−0.019	0.044
5183.620	$3p\,^3P^o - 4s\,^3S$	0.010	−0.019	0.044
6318.750	$4s\,^3S - 6p\,^3P$	0.005	0.048	0.079
6319.240	$4s\,^3S - 6p\,^3P$	0.005	0.048	0.079
6319.493	$4s\,^3S - 6p\,^3P$	0.005	0.048	0.079
7657.600	$4s\,^3S - 5p\,^3P$	0.008	0.060	0.135
$\overline{\Delta \log \varepsilon}$		0.007	0.035	0.069
$\sigma_{(n-1)}(\log \varepsilon)$		0.014	0.021	0.027
$\sigma_{(n)}(\log \varepsilon)$		0.015	0.022	0.028

the additional differentiation of excitation energies to produce acceptable line fits.

5. Discussion

The results of the non-LTE calculations from various Mg I lines shown in Table 2 confirm that deviations from LTE of the level populations of neutral magnesium are quite small in the Sun. The resulting effects on line formation are almost negligible in the visible solar spectrum. We find that only lines in the infrared show a significant non-LTE effect. The singlet lines at $\lambda\lambda$ 8806, 8923 and 11828 Å begin to show significant deviations from LTE at the line cores. A Mg I atomic model *without* neutral hydrogen collisions probably cannot reproduce the observed profiles of these lines. The lines at 12μm allow the best discrimination between the models, they cannot be fitted when the hydrogen collisions are too strong. In fact, the additional exponential dependence on excitation energy of the hydrogen collisions obtained by applying a cross-section significantly reduced with respect to Drawin's (1969) formula produces the most realistic profile centres, and the 12μm line emission lines at the solar limb are also well reproduced. The interacting levels of the Mg I atom in the solar photosphere are well respresented by our choice of lines analyzed, with the principal levels below 6 eV included. All lines in the blue, notably multiplets 12 to 16 are heavily blended, and there will be no loss of information due to excluding these lines. Lines in the infrared are combining even higher excited levels of which we have only analyzed the 12μ lines to put strong limits on the hydrogen collison rates. Thus we do not expect to improve the calculations significantly by comparison with additional IR lines that have been observed in the solar spectrum. The question of how reliable our results are must be answered with respect to our choice of free parameters. Since we have used *standard formulae*, each with only 1 or 2 parameters to fit, we are confident that our atomic model is well determined.

The present investigation will serve as a basis for further analyses of the statistical equilibrium in metal-poor stars, and it is interesting to estimate the changes expected with reduced metallicity. With the density of free electrons decreasing in proportion to the star's metal abundance we expect considerably reduced collisional interaction. This could lead to substantially stronger deviations from LTE at optical depths log τ_c between -3 and 0, if the reduced electronic interaction is not compensated by hydrogen collisions (Baumüller & Gehren, 1996, 1997). Corresponding calculations will be presented in a forthcoming paper.

Acknowledgements. This research was supported by the Deutsche Forschungsgemeinschaft and the National Natural Science Foundation of China. We thank Dr. J. Brault who kindly provided the solar Mg I emission line data in digital form. Our thanks also go to Drs. J. Reetz and D. Baumüller for supporting the line synthesis code, and to Dr. K. Fuhrmann for helpful discussions.

References

Allen C.W. 1973, Astrophysical Quantities, 3rd Edition, Athlone Press, London
Altrock R.C., Canfield R.C. 1974, ApJ 194, 733
Altrock R.C., Cannon C.J. 1972, Sol. Phys. 26, 21
Arnett D. 1991, in Frontiers of Stellar Evolution, ASP Conf. Ser. 20, 389
Athay,R.G., Canfield R.C. 1969, ApJ 156, 695
Auer L.H., Heasley J.N., 1976, ApJ 205, 165
Bates D.R. Damgaard, A 1949, Phil. Trans. R. Soc. London Ser. A 242, 101
Baumüller D., Gehren T. 1996, A&A 307, 961
Baumüller D., Gehren T. 1997, A&A 325, 1088
Brault J., Noyes R. 1983, ApJ 269, L61
Butler K., Giddings J. 1985, Newsletter on the Analysis of Astronomical Spectra No. 9, University of London
Butler K., Mendoza C., Zeippen C.J. 1993, J. Phys. B 26, 4409
Caccin B., Gomez M.T., Severino G. 1993, A&A 276, 219
Carlsson M., Rutten R.J., Shchukina N.G. 1992, A&A 253, 561
Chang E.S., Noyes R.W. 1983, ApJ 275, L11
Chang E.S., Schoenfeld W.G. 1991, ApJ 383, 450
Cowley C.R. 1971, Observatory 91, 139
Dimitrijević M.S., Sahal-Bréchot S. 1996, A&AS 117,127
Drawin H.W. 1969, Z. Physik 225, 470
Edvardsson B., Anderson J., Gustafsson B., Lambert D.L., Nissen P.E., Tomkin J. 1993, A&A 275,101
Farmer C.B., Norton R.H. 1989, A high-resolution atlas of the infrared spectrum of the Sun, NASA Ref. Publ. RP-1224
Freudenstein S.A., Cooper J. 1978, ApJ 224, 1079
Fuhrmann K., Axer M., Gehren T. 1993, A&A 271, 451

Fuhrmann K., Axer M., Gehren T. 1994, A&A 285, 585
Fuhrmann K., Axer M., Gehren T. 1995, A&A 301, 492
Giddings J.R. 1981, Ph.D. thesis, University of London
Gratton R.G., Sneden C. 1987, A&A 178, 179
Hartmann K., Gehren G. 1988, A&A 199, 269
Holweger H., Müller E.A. 1974, Sol. Phys. 34, 57
Holweger H. 1979, in Les Elements et leurs Isotopes dans l'Univers, 22^{nd} Liège Symp., Liège, p. 117
Hunger K. 1960, Z. Astrophys. 49, 131
Kaulakys B. 1985, J. Phys. B 18, L167
Kaulakys B. 1986, Sov. Phys. JEPT, 64, 229
Kurucz R.L. 1990, in Atomic Spectra and Oscillator Strengths for Astrophysics and Fusion, North-Holland, Amsterdam
Kurucz R.L. 1992, Rev. Mex. Astron. Astrofis. 23, 181
Kurucz R.L., Peytremann E. 1975, SAO Spec. Rep. 362
Kurucz R.L., Furenlid I., Brault J., Testerman L. 1984, Solar Flux Atlas from 296 to 1300 nm, KPNO, Tucson
Lambert D.L., Luck R.E. 1978, MNRAS 183, 79
Lemke M., Holweger H. 1987, A&A 173, 375
Lemke M., Holweger H. 1992, A&A 253, 567
Magain P. 1987, A&A 179, 176
Maltby P., Avrett E.H., Carlsson M., Kjeldseth-Moe O., Kurucz R.L., Loeser R. 1986, ApJ 306, 284
Martin W.C., Zalubas R. 1980, J. Phys. Chem. Ref. Data 9, 1
Mashonkina L.I. 1996, in Model Atmospheres and Spectrum Synthesis, eds. S.J. Adelman et al., PASPC 108, 140
Mashonkina L.I., Shimanskaya N.N., Sakhibullin N.A. 1996, Astron. Reports 40,187
Mauas P.J., Avrett E.H., Loeser R. 1988, ApJ 330, 1008
McWilliam A., Preston G.W., Sneden C., Shectman S. 1995, AJ 109, 2736
Meißner K.W. 1938, Ann. d. Physik, 5. Folge, 31, 505
Moccia R., Spizzo P. 1988, J. Phys. B 21, 1121
Murcray F.J., Goldman A., Murcray F.H., Bradford C.M., Murcray D.G., Coffey M.T., Mankin D.G. 1981, ApJ 247, L97
Omont A. 1977, Journ. de Phys. 38, 1343
Peach G. 1967, Mem. R. Astron. Soc. 7, 1
Petitjean L., Gounand F. 1984, Phys. Rev. A 30, 2946
Regemorter H. van 1962, ApJ 136, 906
Rutten R.J. 1988, in Cool Stars, Stellar Systems and the Sun, ed. G. Wallerstein, PASPC 9, 91
Seaton 1962, in Atomic and Molecular Processes, ed. D.R. Bates, New York Academic Press, p.374
Steenbock W. 1985, in Cool Stars with Excesses of Heavy Elements, eds. M. Jaschek and P.C. Keenan, Reidel, Dordrecht, p. 231
Stürenberg S., Holweger H. 1990, A&A 237, 125
Thielemann K.F., Nomoto K., Hashimoto M. 1996, ApJ 460, 408
Wallerstein G. 1961, ApJS 6, 407
Wiese W.L., Smith M.W., Miles B.M. 1969, NBS Ref. Data Ser. NSDRS-NBS 22
Woosley S.E., Weaver T.A. 1995, ApJS 101, 181
Zirin H., Popp B. 1989, ApJ 340, 571

This article was processed by the author using Springer-Verlag LaTeX A&A style file *L-AA* version 3.